MTMW20 Portfolio 3

Climate Change and ENSO

March 2023

1 Introduction

ENSO's is one of the most dominant modes for interannual climate variability, and so understanding its variation under global warming is crucial for informing adaptation and mitigation strategies. The delayed action oscillator model (DAO), originally proposed by Suarez and Schopf (1988), is one of the several viable frameworks for replicating ENSO dynamics. In this analysis, a Python implementation of the DAO model developed by Charlton-Perez (2012) is used, with underlying theory elaborated in the accompanying class notes.

This study aims, firstly, to implement extensions to the DAO model in accordance with those detailed by Boutle et al. (2007). Subsequently, these extensions are used to explore the expected shifts in ENSO characteristics under various warming scenarios. Properties under consideration include the dominance of El Niño and La Niña regimes, the interaction between the initial Kelvin wave and solar cycle, and the frequency of ENSO events.

2 Model Configuration

The following section provides an overview of the configuration of the provided DAO model, along with the additional forcings incorporated.

2.1 Nondimensionalisation

Boutle et al. (2007) presents the DAO model as a non-linear differential equation in the dimensionalised form:

$$\frac{dT}{dt} = kT - bT^3 - AT(t-\Delta) + \frac{dY}{dt} + \beta + R(t) \tag{1}$$

with T, the temperature anomaly, Δ, the transit time of the Kelvin wave, A, the strength of the returning delayed signal relative to the local non-delayed feedbacks, Y, the annual solar cycle, β the imposed warming in units $^\circ C/100$ years, and $R(t)$, the temperature anomaly due to stochastic wind forcing.

Using the relations $t = t'/k$ and $T = \sqrt{k/b}T'$, the model is implemented in its non-dimensionalised form:

$$\frac{dT^{'}}{dt'} = T - T^3 - \alpha T(t-\delta) + k\sqrt{\frac{k}{b}}\left(\frac{dY}{dt} + \beta + R(t)\right) \tag{2}$$

Throughout the analysis, it is assumed that $b \approx k$.

2.2 Visualisation

The temperature anomaly output from the DAO model, subsequently termed the composite anomaly, is computed for $\Delta t = 400$ days and $\alpha = 0.7$, over a duration of ~ 27 years. The composite profile, as well as the profiles of the model's individual components, including the annual solar cycle, monthly

stochastic wind forcing cycle, and the initial Kelvin wave oscillation, are shown in Fig. 1. The solar and wind cycles are depicted for one period only.

The solar cycle is configured in accordance with Boutle et al. (2007) as a sine wave with an amplitude of $\pm 0.6°C$, attaining a minimum in January and December, and peaking in June. Despite its relatively modest amplitude relative to the stochastic forcing, its derivative has a larger magnitude of the order $4°C$, and thus it is a significant contributor in Eq. 2.

The stochastic wind cycle updates to a randomly distributed value every 30 days, with a mean of $0°C$ and a standard deviation of $5°C$ in accordance with Boutle et al. (2007). Its amplitude typically fluctuates within a range of $\pm 15°C$, making it a significant source of short-term variability in the model.

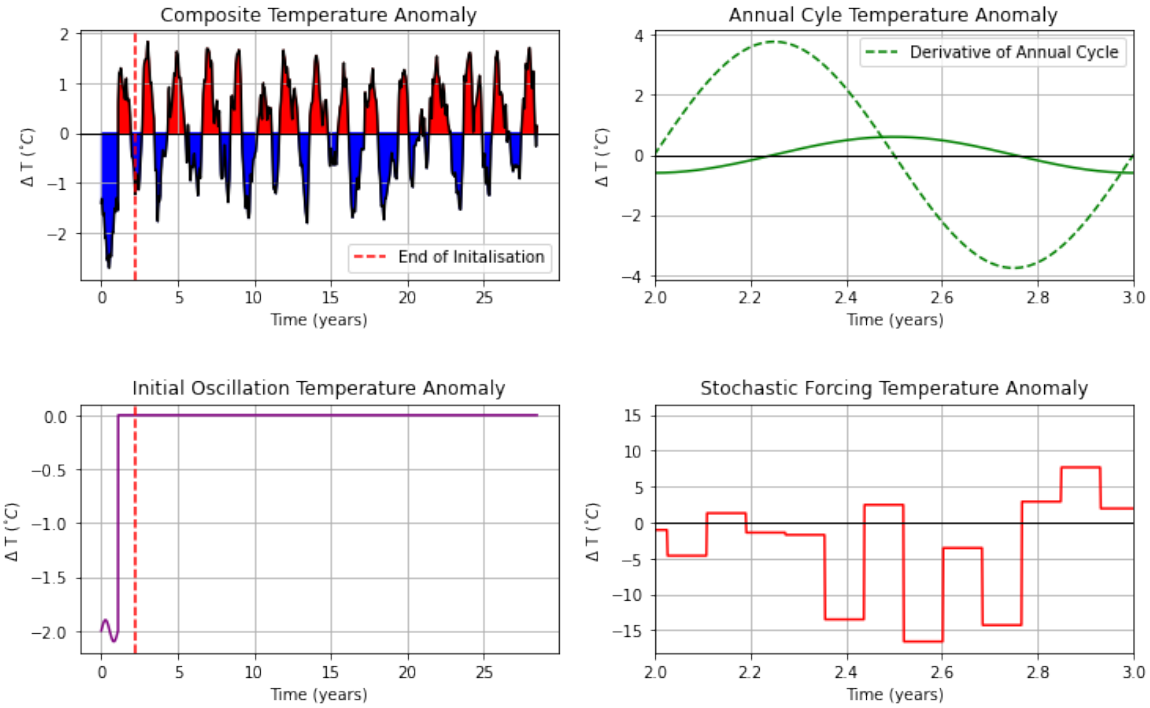

Figure 1: Temperature anomaly profiles derived from the DAO model output and its components. In the top right panel, the equatorial solar cycle is depicted over a single period. In the bottom right panel, the stochastic wind forcing is shown over the same cycle, updating every 30 days. The bottom left panel depicts the initial oscillation of a Kelvin wave. The end of the initialisation period is marks the wave's full reflection, indicated by a dashed red line. The composite anomaly profile output is shown in the top left panel, with El Niño and La Niña phases highlighted in red and blue, respectively.

The initial oscillation, of the Kelvin wave, pre-configured in the provided Jupyter notebook, has an amplitude of $-2 \pm 0.1°C$. Upon the complete reflection of the Kelvin wave, the initialisation period concludes, and the model output is presumed to be stable.

The resultant composite temperature anomaly in Fig. 1 consists alternating El Niño and La Niña phases, marked by varying intensity and duration over time. It bear a striking resemblance to the observed ENSO 3.4 Index profile, especially in terms of magnitude.

3 Results & Analysis

In the following section the effects of varying the model input parameters are assessed within the context of global warming.

3.1 Phase Dominance

A regime characterised by El Niño 'dominance' can be identified by a greater time-integrated area above the x-axis, with the opposite true for La Niña dominance. Such dominance typically correlates with higher peak intensity and/or prolonged peak duration, without distinguishing between the two.

Initially, the area above and below the x-axis is integrated over a ~ 27 year period (not shown), using the parameters outlined for Fig. 1, with the exclusion of the annual cycle and stochastic wind forcing. For β within a range of $\pm 10°C/100$ years, a critical warming of approximately $8.0°C/100$ years is observed over this period, beyond which El Niño becomes increasingly dominant.

When re-simulated over 100-years, the critical threshold emerges at $\beta = 3.1°C00$ years, as illustrated in Fig. 2. Visual inspection of the of the composite profiles for both the 27- and 100-year integrations reveal a a dominance that is not highly discernible, although slightly clearer in the latter case, which is shown in Fig. 2 for $\beta = 10°C/100$ years.

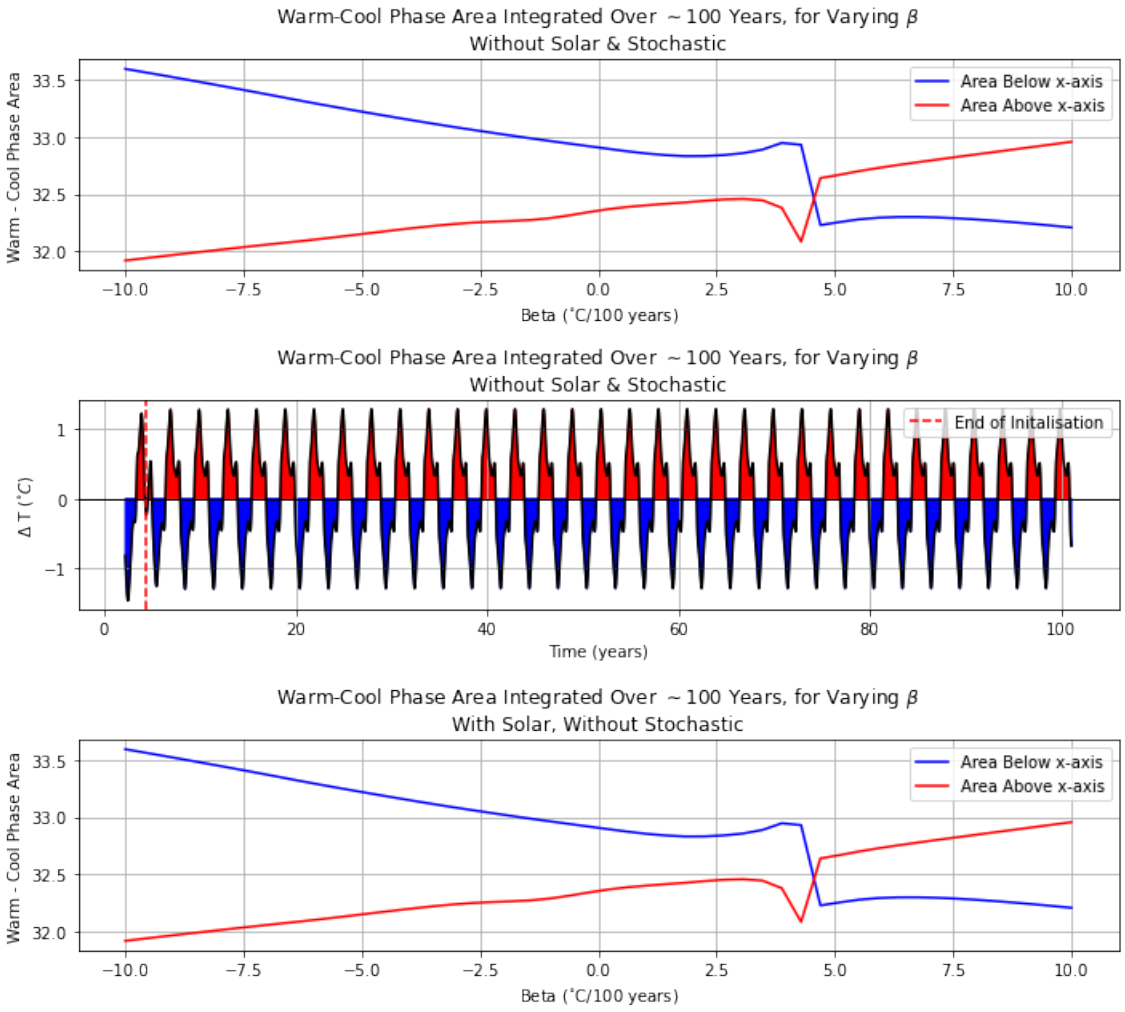

Figure 2: The area above and below the x-axis in the DAO composite temperature anomaly profile is integrated over a 100-year period, for various values of β. The top panel illustrates this integration without the inclusion of the solar and stochastic cycles, while the bottom panel includes only the solar cycle. The center composite profile is depicts the former under $\beta = 10°C/100$ years, demonstrating the subtlety of the El Niño dominance.

Interestingly, when the annual cycle is included, shown in the bottom panel of Fig. 2, the critical threshold increases to $4.6°C/100$ years. When stochastic forcing is also included, the dominance

oscillates between El Niño and La Niña, with no one critical point apparent. Given that various studies (Liu, 2012; McGregor et al., 2009; Awo et al., 2016) have highlighted stochastic wind forcing as the dominant mode of interdecadal climate variability in ENSO, the absence of a clear pattern warrants further consideration.

This method alone is not sufficiently comprehensive to quantify temporal warming patterns. The analysis reveals a general warming trend over the specified time frame, but does not assess the significance of this warming in the broader context of climatology, or indicate the critical time frame at which an ENSO phase begins to dominate under a given β.

Hence, the conclusions drawn from this methodology should be primarily qualitative. They indicate that the effects of a forced warming, such as global warming, may only manifest over extended time scales. A warming of $4.6°C/100$ years over the Pacific in the next century could potentially initiate a transition in the ENSO system towards El Nino dominance. This is concerning, as it aligns with the upper-end range of global SST increase predicted by the SSP2-4.5 'middle of the road' scenario.

3.2 Initial Oscillation Delay

When incorporating the solar cycle into the model, it is crucial to consider the timing of the Kelvin wave, as its reflection can interfere with the solar cycle anomaly. To investigate this phenomenon, a delay is introduced in the onset of the Kelvin signal, and the model is modified to ensure a complete initialisation period. Given that the solar cycle evolves over Milankovitch cycles of the order ¿ 10 ka, its onset and duration are assumed to remain constant over time.

Using the same parameters as described in Section 3.1, the difference in area above and below the x-axis is computed over the 27 year period. Positive and negative values signify El Niño and La Niña dominance, respectively. This computation is repeated for delays in the range $0 - 365$ days. The resulting data are presented in Fig. 3, organised into 2 subplots based on their distinctive characteristics.

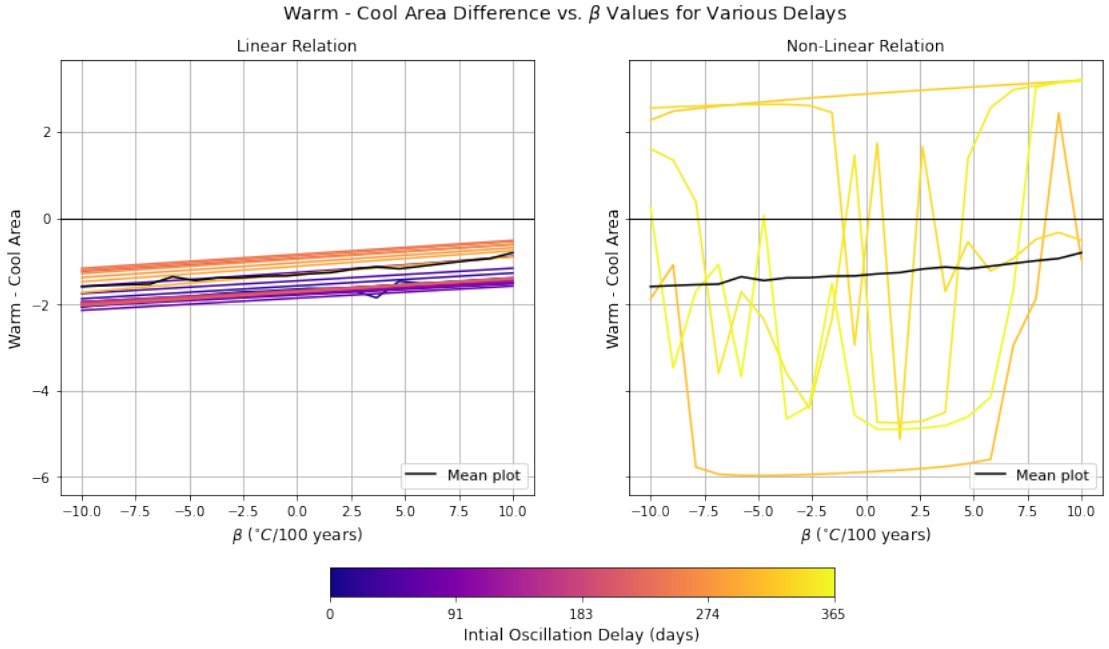

Figure 3: The difference between the area above and below the x-axis in the DAO composite temperature profile is computed over a ~ 27 year period, for various values of β and Kelvin wave delays. The resulting plots are organised into those with a linear relationship, and those with a non-linear relationship attributed to lag-switching. The black line represents the mean trend across all plots, derived from a high-resolution simulation.

The left panel features the majority of simulations, marked by a primarily linear trend: decreasing La Niña dominance with increasing β. The right panel contains fewer simulations, which oscillations between El Niño and La Niña dominance, with no clear pattern evident across the range of β or delay values. It's worth noting that these plots were simulated within the upper delay range, spanning from $300 - 365$ days. This aspect is further discussed in the following section.

The black plot depicted in Fig. 3 represents the average trend derived from a high-resolution simulation. Given the continuous emission and reflection of Kelvin waves, and assuming no temporal bias, this plot reflects the mean impact of the Kelvin waves. Over the integration period, La Niña dominates while $\beta < 10°C/100$ years. However, as β increases, this dominance gradually transitions towards El Niño conditions. While performing the integration over a century may provide more insights, this would require a lengthy computational run time. Nonetheless, it is anticipated that the findings from an extended simulation would align with those of Section 3.1.

3.3 Dominance-Switching

The Kelvin wave, with a period of 400/365 days or approximately 1.1 years, and the solar cycle, with a period of 1 year, both follow sine wave patterns oscillating in the same direction. Introducing a delay of approximately $\sim$ 330 days compensates for the Kelvin wave's longer period, initially aligning the two waves in-phase after one period of the Kelvin wave. However, their phase difference gradually accumulates over time. Although this observation is intriguing and likely relevant, it alone does not account for why delays within this specific range lead to the non-linear relation observed in Fig. 3.

To explore this further, a cross-correlation is conducted between the composite anomaly and the interference signal generated by the initial oscillation and the solar cycle anomalies. From this analysis, the point of maximum (positive) correlation is determined, and the associated time lag between the composite and interference signals is determined. A negative lag indicates that the interference signal leads the composite signal, and vice versa for a positive lag. These lags are calculated for each combination of β and delay pairs in Fig. 3, and plotted in Fig. 5 in the Appendix.

By observing the movement of data points within the plot, it becomes evident that, for example, with a delay of 100 days, the time lag remains approximately constant and negative as β varies. However, for delays of 225, $300 - 315$, or $328 - 365$ days, when β is varied, the lag between the two signals oscillates between its original negative value and a positive value approximately double in magnitude. This lag-switching phenomenon appears to correspond to the dominance switching pattern observed in Fig. 3.

3.4 Power Spectra & Frequency

In this section, the power spectra and the frequency of El Niño and La Niña events are examined under the same parameters as Section 3.1. The power spectra are produced under three conditions: without the solar or stochastic cycle, with only the solar cycle, and with both cycles included. This analysis spans various values of β, with no delay assumed for the solar cycle.

The mean frequency corresponding to the maximum of the power spectrum, computed across the range of β values, remains consistent regardless of the presence of the solar cycle, with a negligible standard deviation. However, the power at this frequency reduces for all β values upon the inclusion of the solar cycle.

Furthermore, the introduction of the stochastic cycle results in a decrease in the mean frequency at the maximum power and an increase in its standard deviation. Moreover, the variance of the power at this frequency also increases significantly.

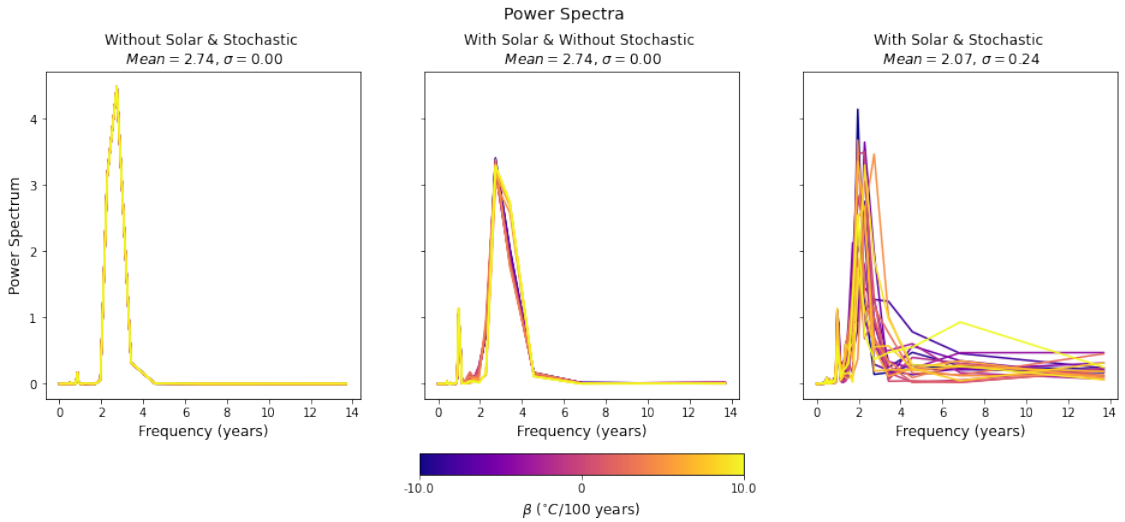

Figure 4: Power spectra produced for various β values over a ~ 27 year period. This is conducted for the raw DAO model (left), with the addition of the solar cycle (centre), and the addition of both the solar cycle and stochastic wind cycle (right).

These findings suggest that the inclusion of the annual cycle, along with variations in the warming parameter magnitude, does not lead to a significant change in the dominant frequency of ENSO events from 2.7 years. However, the addition of stochastic forcing tends to reduce this dominant frequency to approximately 2.2 years. In this scenario, the oscillation period becomes twice the input transit time (1.1 years), a phenomenon known as period-doubling bifurcation.

Despite the decrease in mean frequency, the stochastic forcing increases the power of higher frequency events. ENSO events typically occurs in cycles ranging from $2 - 7$ years, suggesting that stochastic wind forcing is crucial accurately replicating real-world dynamics.

Interestingly, across all three cases, no clear relationship between the dominant frequency and β is discernible. Several climate model studies, including Cai et al. (2014), propose that El Niño events could become more frequent as temperatures rise. This points to a potential limitation of the DAO model in capturing this dynamic.

3.5 Phase Space

For the long-term variability of the DAO model, especially global warming, the phase dynamics must be considered. The model can be represented in phase space as the rate of change of the composite anomaly against the composite anomaly.

A stable phase space implies that the trajectory neither grows nor decays over time. Similarly, pseudo-stability suggests that the phase continuously oscillates between growth and decay regions while remaining on the same trajectory overall.

Ideally, the parameterisations used throughout the analysis, namely α and Δ, maintain stability in phase space irrespective of the applied β. For $\alpha = 0.7$ and $\Delta = 400$ days, the system remains stable even under unlikely warming scenarios of $1°C/$ year.

Boutle et al. (2007) provides a phase diagram delineating the stable and unstable regions for various Δ-α combinations.

4 Conclusion

The simplicity of the DAO model offers a unique opportunity to explore the implementation of various forcings, as demonstrated in this analysis. Despite its simplistic nature, the model has

yielded valuable insights into expected shifts in phase dominance, the interaction between Kelvin and solar cycles, and event frequency under different warming scenarios.

The analysis conducted suggests that a warming exceeding $\sim 4.6°C$ over the next century would likely promote El Niño dominance, whereas a lesser warming trend would coincide with La Niña dominance.

Moreover, the model offers a compelling avenue for examining the role of interference, although its significance within the context of global warming is likely averaged out. Investigation into the power spectrum unveils a limitation of the model, prompting consideration for an extensions of the analysis to ascertain whether this limitation persists across other ENSO frameworks, such as the recharge oscillator model.

Overall, these findings underscore the need for a more comprehensive methodology and a deeper exploration into the role of stochastic forcing within the DAO.

References

Suarez, M. J., & Schopf, P. S. (1988). A delayed action oscillator for enso. *Journal of the Atmospheric Sciences*, *45*, 3283–3287. https://doi.org/10.1175/1520-0469(1988)045⟨3283:ADAOFE⟩2.0.CO;2

Charlton-Perez, A. (2012). Dao.py.

Boutle, I., Taylor, R. H. S., & Römer, R. A. (2007). El niño and the delayed action oscillator. *American Journal of Physics*, *75*, 15–24. https://doi.org/10.1119/1.2358155

Liu, Z. (2012). Dynamics of interdecadal climate variability: A historical perspective. *Journal of Climate*, *25*, 1963–1964. https://doi.org/10.1175/2011JCLI3980.1

McGregor, S., Holbrook, N. J., & Power, S. B. (2009). The response of a stochastically forced enso model to observed off-equatorial wind stress forcing. *Journal of Climate*, *22*, 2513. https://doi.org/10.1175/2008JCLI2387.1

Awo, F. M., Alory, G., & Baloïtcha, E. (2016). The delayed oscillator model for climate variability: A review and an application to the atlantic meridional mode. *Environmental Modelling and Software for Supporting a Sustainable Future, Proceedings - 8th International Congress on Environmental Modelling and Software, iEMSs 2016*, *1*, 1–8.

Cai, W., Borlace, S., Lengaigne, M., Rensch, P. V., Collins, M., Vecchi, G., Timmermann, A., Santoso, A., Mcphaden, M. J., Wu, L., England, M. H., Wang, G., Guilyardi, E., & Jin, F.-F. (2014). Increasing frequency of extreme el niño events due to greenhouse warming, 111. https://doi.org/10.1038/NCLIMATE2100

5 Appendix

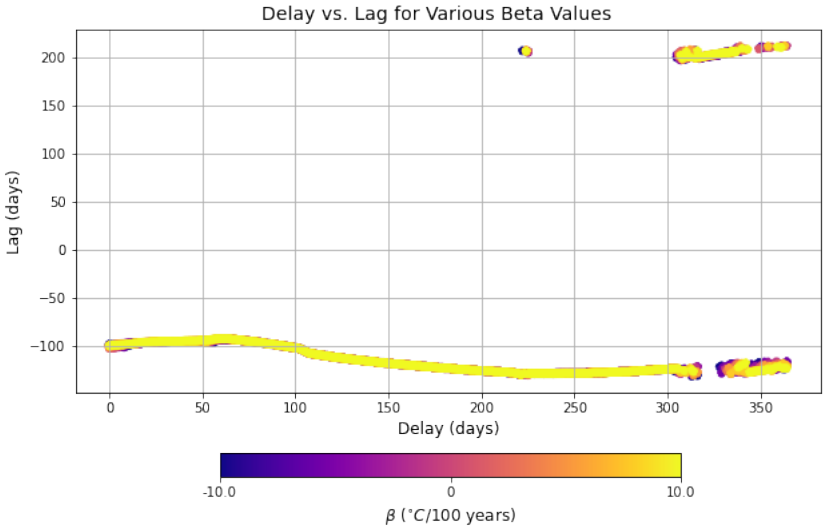

Figure 5: A cross-correlation analysis is performed on the plots depicted in Fig. 3 to determine the time lag between the interference and composite signals. The resulting time lag is plotted, revealing a lag-switch phenomenon upon varying β at a fixed initial oscillation delay.

1975 words = 4 PU; 4 images = 4 PU; Total = 8 PU